A constitutive model for semi-crystalline polymers at high temperature and finite plastic strain: Application to PA6 and PE biaxial stretching

Fanfei Zeng, Philippe Le Grognec, Marie-France Lacrampe, Patricia Krawczak

A constitutive model for semi-crystalline polymers at high temperature and finite plastic strain: Application to PA6 and PE biaxial stretching

Fanfei Zeng, Philippe Le Grognec *, Marie-France Lacrampe, Patricia Krawczak

Univ. Lille Nord de France, F-59000 Lille, France
Ecole des Mines de Douai, Polymers and Composites Technology and Mechanical Engineering Department, 941 rue Charles Bourseul, BP 10838, F-59508 Douai, France

This paper deals with the mechanical behavior of semi-crystalline polymer films at high temperature (90 °C) in finite plastic strains. Due to the complex morphology of such mate-rials, standard elastoplastic formulations are not suitable for describing in a unified way their uniaxial and biaxial tensile behaviors which involve specific physical phenomena. According to physical considerations concerning the mesoscopic semi-crystalline structure of such polymers, a constitutive model has been specially developed, with the idea of a three-phase morphology in relation to the average distance between crystalline blocks. A quite classical constitutive law is used to describe the mechanical (hyper)-elastic and/or plastic behavior of each phase (an eight-chain "network" model is employed). As a key of the work, a "multi-axial factor" is introduced, in the context of perfect plasticity, so as to relate the threshold stress and the deformation mode, considering the effect of entangle-ments. Uniaxial and equi-biaxial tensile experimental tests have been performed using two materials: polyamide 6 and polyethylene. Model parameters are calibrated using uniaxial stress–strain experimental curves. Then, the biaxial simulation curves are shown to be in very good agreement with the corresponding experimental results.

1. Introduction

Polymer films for food packaging are very convenient and widely applied in everyday's life. However, these consumer products must respond simultaneously to so many performance criteria (impermeability to liquids and gas, mechanical strength, transparency) that the use of a single polymer does not generally meet the specifications required for this type of application. Therefore, in most cases, polymer films are made from several polymers, each of which bringing an interesting property to the combination thus formed. For example, the combination of polyamide 6 (PA6) and polyethylene (PE) has shown a particular interest for combining the good mechanical strength and impermeability to gas (e.g. O_2) of PA6 with the high ductility and impermeability to liquids (e.g. H_2O) of PE.

Modeling the mechanical behavior of such multi-layer films, especially in uni- and biaxial stretching under high temperatures which is supposed to improve the mechanical properties, is therefore an important objective for industrial applications. This knowledge is related to the establishment of a constitutive model for each polymer material that can account for large irreversible deformations and reproduce in a unified way the uni- and biaxial behaviors.

In recent years, many authors investigated the mechanical behavior of semi-crystalline polymers, following different points of view, from the physical description of

* Corresponding author at: Ecole des Mines de Douai, Polymers and Composites Technology and Mechanical Engineering Department, 941 rue Charles Bourseul, BP 10838, F-59508 Douai, France. Tel.: +33 3 27 71 23 21; fax: +33 3 27 71 29 81.

E-mail addresses: fanfei.zeng@mines-douai.fr (F. Zeng), philippe.le.grognec@mines-douai.fr (P. Le Grognec), marie-france.lacrampe@mines-douai.fr (M.-F. Lacrampe), patricia.krawczak@mines-douai.fr (P. Krawczak).

the morphology at various scales to the numerical simulation of the macroscopic behavior possibly relying on physical considerations.

On one hand, several studies were based on micrographic observations and aimed at depicting the structure of such polymers, in order to better explain their overall behavior. For example, Boni et al. (1982) and Aboulfaraj et al. (1995) discovered a variety of spherulitic morphologies composed by lamellae of crystalline phase in polybutene and polypropylene, respectively. In high-density polyethylene, ringed spherulites were also surveyed using an optical microscope, as mentioned in Peacock (2000). Furthermore, Heck et al. (2000) observed several semi-crystalline polymers, among which poly-(ethylene-co-octene)s and polypropylenes, and measured the average size of crystal blocks which was found to be the minimum value ensuring the stability of the crystalline structure. The experimental achievement of micro-structural parameters such as the crystallinity, the orientation and size factors of each phase, allowed Fatahi et al. (2007) to correlate the tensile modulus of polyethylene blown films with their physical characteristics.

Referring to experimental stress–strain tensile curves, it was often reported in the literature that semi-crystalline polymers sometimes exhibit a double yielding point. The influence of structural morphology such as the degree of crystallinity or the lamellae thickness, and external factors, such as temperature or strain rate, on the occurrence of a double yield point was analyzed by many authors (among which Balsamo et al. (1993) and Feijoo et al. (1997) dealing with various polyethylenes and their blends), who tried to understand this particular feature in different ways. Several micromechanical processes were suggested. Among others, Séguéla and Rietsch (1990) proposed that the two yield points were due to the slip of the crystal blocks past each other in the mosaic crystalline structure (heterogeneous slip) and the homogeneous shear of the crystal blocks (homogeneous slip). Considering polyamide 6 composites, Shan et al. (2005) showed that the change of crystalline structure was one of the main mechanisms involved in the formation of a double yield point. They proved that a double yielding phenomenon is more likely to occur with low crystallinity ratios and low strain rates.

On the other hand, many constitutive models were proposed to simulate the mechanical behavior of semi-crystalline polymers. A preliminary approach was based on the so-called "network" models, initially developed for elastomers, emphasizing the rubber-like properties of the amorphous phase of semi-crystalline polymers. Rubber-like materials are predominantly defined by an extreme deformability combined with an almost full recovery in unloading procedures. Following these ideas, many network models have been proposed. For instance, one can mention the classical models based on Gaussian statistics or non-Gaussian statistics (e.g. using Langevin distributions) (Kuhn and Grün, 1942; James and Guth, 1943), developed in the context of the statistical mechanics of polymer molecular chains. According to the number of chains employed in the network model with non-Gaussian statistics, one distinguishes the single-chain model (Kuhn and Grün, 1942), the three-chain model, the eight-chain model (Arruda and Boyce, 1993), the p-chain models (James and Guth, 1943) and the full-chain model.

More recently, network models were modified and widely applied in numerical simulations involving amorphous or semi-crystalline polymers (Diani et al., 2004; Richeton et al., 2007; van Dommelen et al., 2003). Let us mention Dupaix and Boyce (2007) who developed a new constitutive model in order to capture the rate-dependent stress–strain behavior of an amorphous polymer (poly-(ethylene terephthalate)-glycol) at and above the glass transition temperature (T_g). These authors particularly considered the effect of intermolecular interactions between neighboring polymer chain segments. Richeton et al. (2007) modified the classical eight-chain model so as to simulate the behavior of poly-(methyl methacrylate) and polycarbonate, taking into account the influence of relaxation in polymer chains. Dealing now with semi-crystalline polymers, the "Arruda-Boyce", "Hasan-Boyce", "Bergström-Boyce" models, and the so-called "Hybrid" model, were developed as a generalization of the eight-chain model for predicting the large strains, time- and temperature-dependent elastoplastic response of ultra-high molecular weight polyethylene, as reviewed in Bergström et al. (2002). Gueguen et al. (2008), as well as Lee et al. (1993) and van Dommelen et al. (2003) in a different way, investigated the elasto-(visco)-plastic behavior of semi-crystalline polymers using a micromechanically-based formulation, considering two phases (crystalline and amorphous) with independent yield processes. Hong (2005) constructed a specific model for the simulation of various kinds of polyethylene (e.g. linear polyethylene, branched polyethylene, poly-(ethylene-co-vinylacetate)) under uniaxial tension. Two models were used in parallel to represent the combined effect of amorphous chains and crystalline skeleton (see also Hong et al. (2004)). A homogenization procedure was also applied in Drozdov and Christiansen (2008) in order to predict the thermo-viscoelastic and viscoplastic behavior of high-density polyethylene, but considering not only two but three different phases, with an inter-phase at the interface between crystalline and amorphous phases.

Although many models have been proposed so far and validated with uniaxial experimental tests, their use in the case of a biaxial tensile behavior has rarely been investigated until now. In this paper, a special model is introduced, partly based on the constitutive models discussed above, which is intended to catch both uniaxial and biaxial behaviors of semi-crystalline polymers, where standard elastoplastic models naturally failed. The general idea of the present model results from the three-phase description of the morphology of the extruded films considered, in relation to the average distance between crystalline blocks, and of the physical description of their mechanical behavior. On one hand, somewhat classical hyperelastic and plastic models are employed for the two phases corresponding to the extreme distances between crystalline blocks. On the other hand, the third model related to the intermediate phase includes, in the context of perfect plasticity, a "multi-axial factor", so as to relate the threshold stress and the deformation mode, considering the effect of entanglements.

Eventually, the objective is to consider explicitly the crystalline structure and the global morphology of the extruded films. Nonetheless, it is convenient to confirm first the capability of such a model to reproduce the macroscopic response of the films in uniaxial and biaxial drawing. This is the framework of the present work, which is not concerned with the correlation between the model parameters and the crystallinity of the materials (whose identification is out of the scope of this study and will be performed later). Thereby, for the two materials considered (polyamide 6 and polyethylene), uniaxial and equibiaxial tensile experimental tests will be performed. The uniaxial stress–strain experimental curves are used to calibrate the model parameters. Then, the biaxial simulation curves will be compared with the corresponding experimental results, in order to evaluate the efficiency of the present model.

2. Morphology of semi-crystalline polymers

The mechanical behavior of a semi-crystalline polymer is strongly influenced by its morphology. Thus, a quick presentation on the physical structure of semi-crystalline polymers is first carried out in order to better explain the macroscopic properties of these materials observed in experimental testing and justify the subsequent choice of the different components of the future model.

Polymers are macro-molecules which are composed of giant chains in repeated patterns of molecular sequences connected by covalent bonds. The molecular shape and the way by which molecules are arranged in the solid state are important factors for the determination of the physical and/or mechanical properties of polymer products. In crystalline materials, molecules are perfectly arranged in repeated patterns. Such materials display an highly ordered and regular structure. In amorphous materials, by contrast, molecules are randomly arranged in long chains which twist and curve around one another, so that large regions of highly structured morphology are very unlikely. In between, semi-crystalline polymers (like PA6, PE, and most polymers) consist in mixtures of small crystals in an amorphous medium.

As shown in Fig. 1a, which describes a morphological model of polypropylene (Peacock, 2000), semi-crystalline polymers can be viewed as three-phase materials, including interfacial regions between successive crystalline and non-crystalline zones. This simple model is still used by many authors, among which Drozdov and Christiansen (2008) and Hong et al. (2004), and it will be retained for our materials. Interfacial regions are about 10–30 Å thick, depending on the polymer and crystallization conditions, and can comprise up to 30% of the matter for medium to high molecular weight materials (Mandelkern, 2006). Moreover, the thickness of the non-crystalline regions is about 50–200 Å, whereas the average extended length of a typical polyethylene molecule is 1 μm (Peacock, 2000).

As reviewed in Hong (2005), when the volume fraction of crystallites is higher than 10% (which is the case for the materials used in this study, see Table 1), these crystallites form a lamellar structure (the crystallization of homopolymers such as polyethylene from a dilute solution is lamellar-like) and experimental observations show that the lamellar crystals are arranged in arrays of blocks, as shown in Fig. 1b. The thickness of lamellae is of the order of 80–200 Å.

It can thus be assumed that semi-crystalline polymers are merely composed of many crystalline blocks which are almost randomly distributed in an amorphous medium, so that the material appears to be almost homogeneous at the macroscopic scale. However, the links between crystalline blocks and the surrounding amorphous region may greatly influence the mechanical behavior. Three scenarios will be distinguished in the sequel: a first case where crystalline blocks are inter-connected by very short intra-lamellar chains and two other cases involving the inter-lamellar distance which is assumed to be either middle-sized or rather long.

3. Experimental procedure and results

Two materials are considered in this study. The first one is a non-nucleated grade of polyamide 6 (PA6) provided by DSM (Geleen, Netherlands, reference AKULON F236C). The second one is a blend of 30 wt% of low-density

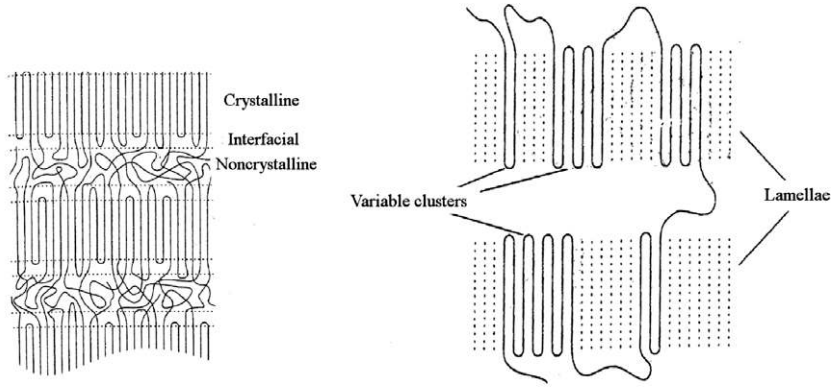

(a) A three-phase representation of polyethylene

(b) Variable cluster model

Fig. 1. Morphology of semi-crystalline polymers (Peacock, 2000).

Table 1
Thermal properties of PA6 and PE (Sallem-Idrissi, 2008).

Polymer	Glass transition temperature (°C)	Melting temperature (°C)	Crystal weight fraction (%)
PA6	48	220	25 ± 1
PE	−78	120	40 ± 5

polyethylene (LDPE, reference 2101TN00) and 70 wt% of linear low-density polyethylene (LLDPE, reference 118 N) both provided by SABIC. The films were manufactured by extrusion blowing with a constant thickness of 100 μm. FTIR experiments have indicated a nearly perfect isotropy of the PA6 films, while the PE films exhibit a substantial planar chain orientation induced by the process. Moreover, the crystalline structure of the PA6 films is mainly in the β-form (85%) with a little amount of γ-form (15%). This particular crystalline distribution is induced by rapid cooling during processing. More details on the manufacturing conditions and micro-structure of the films are presented elsewhere (Sallem-Idrissi et al., 2009).

Experimental uniaxial tests are performed using an Instron tensile testing machine together with a conditioning chamber in order to heat the specimens up to the desired temperature (90 °C) and keep it constant during the tests. Considering only isothermal deformations, the temperature will not explicitly appear in the description of our model. The same formulation is however suitable for any other value between the glass transition and the melting temperatures, with elastic or plastic parameters depending implicitly on the temperature. Strains are precisely measured in the dumbbell specimens thanks to an Apollor video-traction system. The biaxial curves used in the sequel come from an earlier experimental work carried out by Sallem-Idrissi (2008). Biaxial stretching experiments were performed on a Cellier tenter frame consisting of four pantographs driven by two hydraulic jacks at right angle, and operated in a temperature-regulated oven. Square specimens were submitted to simultaneous equi-biaxial drawing at a constant jack speed of 60 mm/min (i.e. a strain rate of $9.52 \times 10^{-3}\,s^{-1}$).

Preliminary uniaxial tests are carried out in order to estimate the effect of the loading rate on the stress–strain law. In all the following stress–strain curves, the true logarithmic strains are plotted versus the true Cauchy stresses, which hardly differ from the Kirchhoff stresses, as it will be explained in the next section. As shown in Fig. 2, all the specimens (PA6 or PE) behave similarly for the three following speeds into consideration: 10 mm/min (i.e. a strain rate of $5.55 \times 10^{-3}\,s^{-1}$), 20 mm/min ($1.11 \times 10^{-2}\,s^{-1}$) and 50 mm/min ($2.77 \times 10^{-2}\,s^{-1}$). Viscous effects will thus be neglected in the sequel, since the loading speed does not exceed 50 mm/min, what is verified in practice for our future applications (the minimum value of 10 mm/min will be retained for the following tests).

On one hand, the previous tests prove that these semi-crystalline polymers display an extreme deformability and a strong stress hardening in large strains like elastomers (see Fig. 2). On the other hand, they differ from elastomers because of their elastoplastic irreversible behavior, as shown in Fig. 3 involving cyclic loading curves.

The volume of the specimens are measured at the beginning and the end of each test. It is found to change only very slightly, what agrees with the conclusions of Hong (2005).

Furthermore, some thermal properties of PA6 and PE are listed in Table 1, which may mainly explain the few differences encountered in our experiments between the behaviors of PA6 and PE. Despite these differences, the two materials will be modeled using the same ideas and the same methodology.

Finally, the monotonic uniaxial and equi-biaxial curves are compared for each material in Fig. 4. The double yielding points under uniaxial and biaxial stress states seem to be very different, what can not be explained by using only the classical plasticity theories such as the generalized standard materials theory involving the von Mises criterion, as the corresponding equivalent stress gives the same value in both loading cases.

4. Constitutive model

In this section, a new constitutive model is designed, based on the previous physical and experimental observations. It will then be applied to both cases of PA6 and PE. In this study, due to the very large strains encountered, true logarithmic strains are employed and additively decomposed into elastic and plastic parts, according to the classical Lee multiplicative decomposition of the deformation gradient. Moreover, as volumetric changes are proved to

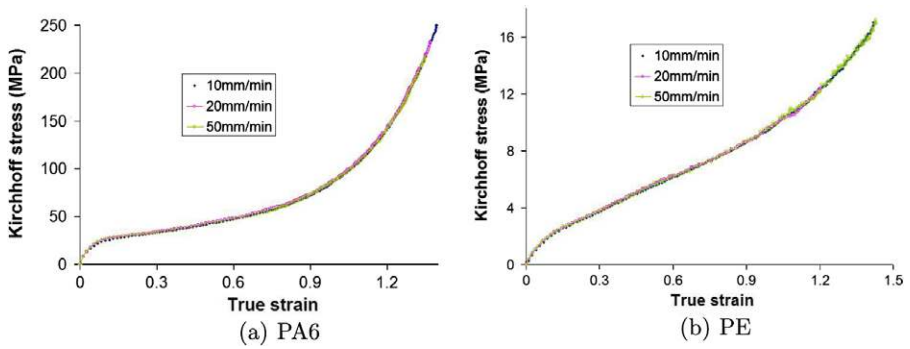

Fig. 2. Uniaxial stretch curves of the semi-crystalline polymers at 90 °C under various strain rates.

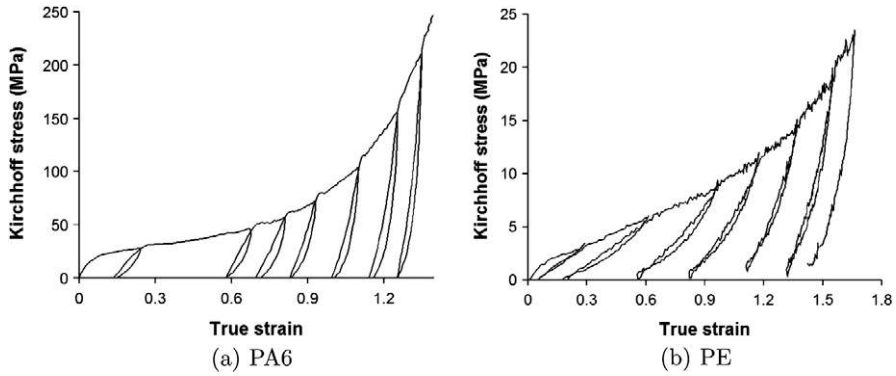

Fig. 3. Loading and unloading curves of the semi-crystalline polymers at 90 °C.

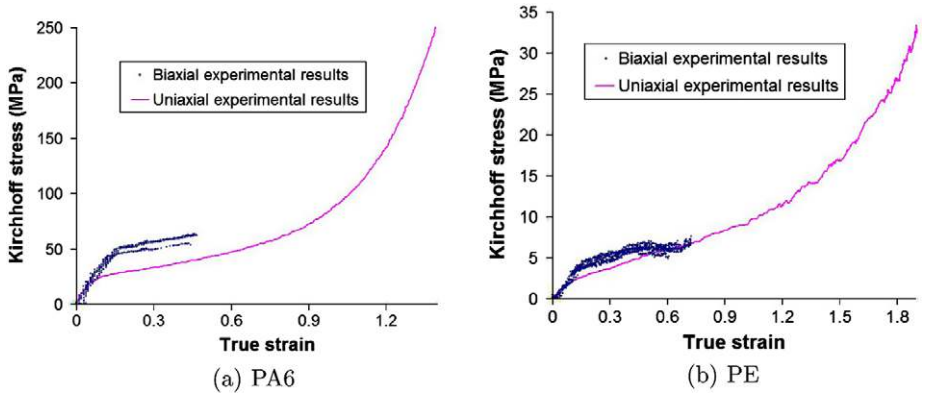

Fig. 4. Comparisons between uniaxial and biaxial experimental curves of the semi-crystalline polymers at 90 °C.

be negligible, the more classical true Cauchy stresses can be employed in place of Kirchhoff stresses (they practically coincide with one another) which should be preferred as a more reliable counterpart of logarithmic strains.

4.1. Basic components of the three-phase model

As shown in Fig. 5, one assumes that a random sample of a semi-crystalline polymer comprises quite a few crystalline blocks connected by molecular chains (standing for the amorphous phase and represented by curved lines). First, the uniaxial drawing of a selected sample typically involves two crystalline blocks linked together with a non-crystalline region. According to the distance between the two blocks, three cases are considered, leading to three particular behaviors.

When the specimen considered is stretched under multi-axial conditions, the representative sample might involve more blocks. The multi-axial behavior will be also discussed in the sequel: it will derive from the uniaxial results by using various criteria partly based on a "multi-axial factor".

4.1.1. Case 1

The distance between the two considered crystalline blocks is very short. Therefore, most chains located between these blocks are connected or even embedded thereto. When the sample is stretched under a uniaxial stress state, the chains within the amorphous region may turn tensile for even a small strain. Once the stress becomes large enough, the chains begin to glide and the material hardens, due to the strong connecting links with the crystalline blocks. The typical uniaxial stress–strain behavior in this case, usually observed with crystalline materials, is depicted in Fig. 6, where E_1 represents Young's modulus, E_{T1} the tangent elastoplastic modulus, and σ_1 is the yield stress of the considered sample.

The generalization to multi-axial stress states is straightforward, in the framework of generalized standard materials, using the von Mises criterion ($\sigma_{VM} = \sqrt{\frac{3}{2}\mathbf{S}:\mathbf{S}}$ with the deviatoric stress tensor $\mathbf{S} = \boldsymbol{\Sigma} - \frac{1}{3}tr(\boldsymbol{\Sigma})\mathbf{I}$ where $\boldsymbol{\Sigma}$ represents the true stress tensor) and an isotropic hardening type. The coupling effects between the elastic and plastic parts of the behavior, clearly observed during unloading (see Fig. 3), will naturally appear with the global model, due to the specific combination of the elementary models employed for each phase.

4.1.2. Case 2

The distance between crystalline blocks is medium-sized. Many chains in the amorphous region are not

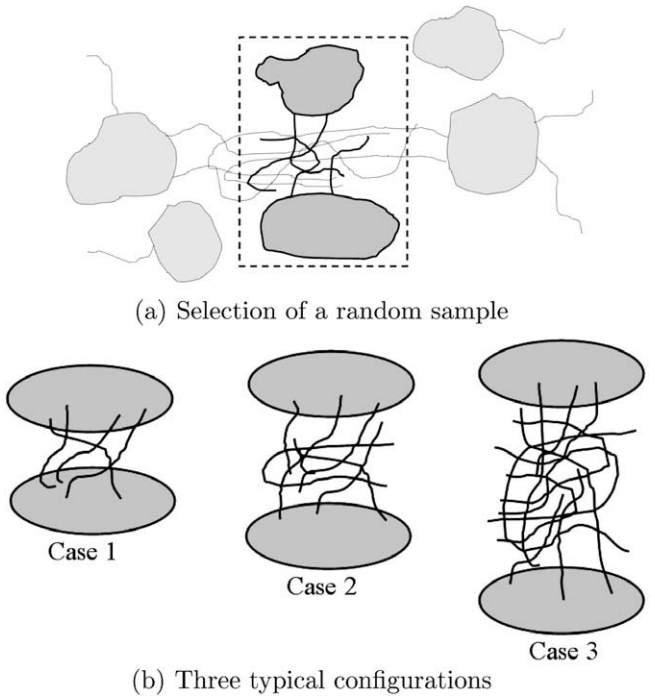

Fig. 5. Distinction of three behaviors according to the distance between crystalline blocks.

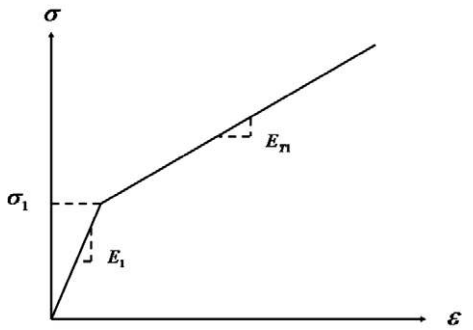

Fig. 6. Stress–strain curve under uniaxial drawing for case 1.

directly connected to all the surrounding crystalline blocks and thus less constrained by their mechanical behavior as compared to case 1. Here, the mechanical response of such a sample is conversely governed by the presence of numerous entanglements between couples of chains.

Isolating two entangled chains at the mesoscopic scale, it is possible to explain their joined mechanical response by the spatial configuration of the couple of chains, namely their relative position and motion. In a macroscopic point of view, due to the huge number of molecular chains involved and their random space distribution, the sample is assumed to behave uniformly. Only the deformation mode (e.g., uniaxial or biaxial) will affect the relative displacements of the chains and consequently the number of entanglements brought into play.

When the sample is stretched uniaxially, the chains in the non-crystalline region tighten rather quickly. Entanglements then naturally appear and a new sliding phenomenon may occur, as the stress increases. All the entanglements are supposed to provide the same contribution to the global resistance against sliding, which is represented by a limit force τ corresponding to the incipient slippage. The macroscopic uniaxial threshold stress σ_2^u (where superscript $.^u$ stands for "uniaxial") resulting from this limit force is therefore proportional to the uniform surface density n^u of entanglements involved in the uniaxial behavior, as follows:

$$\sigma_2^u = n^u \tau \tag{1}$$

In this case, the typical mechanical behavior under uniaxial drawing is expressed as shown in Fig. 7, displaying the yield stress σ_2 defined above (which is also the maximum admissible stress in the context of perfect plasticity) and the elastic modulus E_2 (encompassing the elastic response of both the crystalline blocks and the amorphous phase)

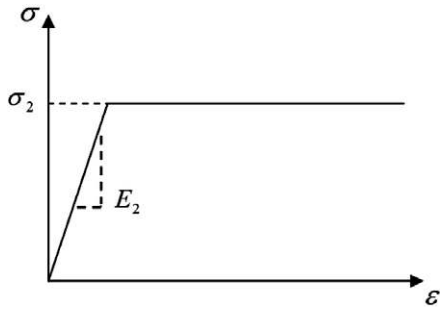

Fig. 7. Stress–strain curve under uniaxial drawing for case 2.

whose influence will further be considered together with the elastic behavior of case 1 in the global model.

Under general loading conditions, one has to replace the uniaxial stress by an equivalent scalar stress function of the multi-axial stress tensor, to be compared to the previous threshold stress. On one hand, the von Mises equivalent stress is used, as the sliding phenomenon is supposed to be governed by shear effects and distortion. On the other hand, a new limit stress is defined, in correspondence with the number of entanglements involved in the multi-axial behavior, which clearly depends on the deformation mode. Let us consider an arbitrary multi-axial strain state and focus on the positive principal strains ε_I which are the ones and only strains in the principal axes that contribute to the interlocking of entanglements. A "multi-axial factor" K is introduced, namely the scaled sum of these strains:

$$K = \frac{\sum_I \varepsilon_I}{\max_I \varepsilon_I} \quad (\varepsilon_I \geqslant 0) \tag{2}$$

The number of entanglements n^m (where superscript $.^m$ stands for "multi-axial") involved in the current multi-axial behavior is then supposed to depend linearly on the parameter K. The associated threshold stress σ_2^m follows the same rules, considering that all the limit forces τ corresponding to each entanglement can be added, regardless of their orientation. In the uniaxial case, Eq. (2) entails $K = 1$, since the strain measured in the loading direction is the single positive value. The following relations are thus obtained:

$$\begin{aligned} n^m &= K n^u \\ \sigma_2^m &= K \sigma_2^u \end{aligned} \tag{3}$$

For the sake of simplicity, a specific modified von Mises criterion is defined, based on the following modified von Mises equivalent stress:

$$\sigma'_{VM} = \frac{\sigma_{VM}}{K} \tag{4}$$

and with a single yield stress σ_2^u which will be further denoted by σ_2. The same modified function is retained for the evolution law, within the framework of associated plasticity.

When dealing with the equi-biaxial tensile test, the "multi-axial factor" takes the value $K = 2$, what means that the number of entanglements involved in the sliding phenomenon is twice as important as in the uniaxial case. Any other biaxial case, when the two relevant positive strains are different one from each other, gives rise to an intermediate value of K. The "multi-axial factor" evolves continuously and even linearly between 1 and 2 corresponding to the two limit cases of uniaxial and equi-biaxial states, respectively.

In practice, dealing with 2D polymer films without any compressive loading in the plane, at least one of the principal strains is strictly positive and the parameter K is always properly defined, except at the reference configuration (the corresponding value can be arbitrarily selected). Moreover, the out-of-plane strain will always be negative, so that only the in-plane deformations will be involved in the calculation of the "multi-axial factor". Nevertheless, let us consider the particular case of a triaxial isotropic stress/strain state. The von Mises type criterion leads to a null equivalent stress σ'_{VM}, independently of the value of K. Indeed, one can easily imagine that both ends of all chains lie in the vicinity of a crystalline block and are equally loaded in such a way that no sliding may occur. Therefore, plasticity is not observed at all in the material.

4.1.3. Case 3

The distance between crystalline blocks is long enough to consider that the chains in the amorphous region are almost unconstrained. In these conditions, a network model such as the eight-chain model is a satisfactory solution to simulate the macroscopic mechanical behavior.

In the 1940's, Kuhn and Grün (1942) and James and Guth (1943) introduced the so-called Langevin model (in the context of non-Gaussian statistics) to deal with large stretches up to the limiting end-to-end distance given by the length of the chains. Considering a molecular chain composed of N monomer segments with length l, its average unstretched length is $l\sqrt{N}$ according to statistical mechanics of freely jointed chains (Elías-Zúñiga and Beatty, 2002), and its total stretched length is lN.

First, a probability density for the stretch distribution in the material is established as follows:

$$P(\lambda) = P_0 \exp\left[-N\left(\frac{\lambda}{\sqrt{N}}\beta + \ln\frac{\beta}{\sinh\beta}\right)\right] \tag{5}$$

with $\beta = \mathscr{L}^{-1}\left(\frac{\lambda}{\sqrt{N}}\right)$, where the inverse of the Langevin function $\mathscr{L}(x) = \coth(x) - 1/x$ cannot be explicitly obtained and is conveniently evaluated by a Padé approximation as mentioned in Miehe et al. (2004):

$$\mathscr{L}^{-1}(x) \approx \frac{(3 - x^2)x}{1 - x^2} \tag{6}$$

Using the Boltzmann's equation (with the so-called Boltzmann's constant k), the strain energy function W of a given chain writes:

$$W = -kT \ln P(\lambda) = NkT\left(\frac{\lambda}{\sqrt{N}}\beta + \ln\frac{\beta}{\sinh(\beta)}\right) - kT \ln P_0 \tag{7}$$

Then, the principle of minimum potential energy leads to the following expression for the stress in a single chain:

$$\sigma = \lambda \frac{\partial W}{\partial \lambda} = \lambda kT\sqrt{N}\mathscr{L}^{-1}\left(\frac{\lambda}{\sqrt{N}}\right) \tag{8}$$

The more recent model based on this approach is the eight-chain model, the eight chains being the half-diagonals of a unit cube. Under the assumption of a constant volume during the loading procedure, namely $\lambda_I\lambda_{II}\lambda_{III} = 1$ (where λ_i ($i = I, II, III$) are the principal stretches), an equivalent stretch is introduced (Miehe et al., 2004; Elías-Zúñiga and Beatty, 2002):

$$\lambda = \sqrt{\frac{\lambda_I^2 + \lambda_{II}^2 + \lambda_{III}^2}{3}} \tag{9}$$

The eight chains being stretched by this same extension ratio, the principal stresses can thus be simply expressed as (Arruda and Boyce, 1993):

$$\sigma_i = -p + \frac{1}{3} C_R \sqrt{N} \frac{\lambda_i^2}{\lambda} \mathscr{L}^{-1}\left(\frac{\lambda}{\sqrt{N}}\right) \tag{10}$$

In Eq. (10), C_R and N stand for the model parameters, accounting for the density and the limit of extensibility of a chain, respectively. These parameters will be further derived from the uniaxial experimental curves (see Section 4.3).

4.2. Full model

At the macroscopic scale, the semi-crystalline polymers considered seem to be homogeneous and roughly isotropic: the amorphous phase is assumed to be randomly distributed around the crystalline blocks and no preferential direction is observed. The structural and mechanical properties of these materials were previously analyzed in Sallem-Idrissi et al. (2009) using methods such as Differential Scanning Calorimetry (DSC), Wide-Angle X-ray Scattering (WAXS) and infrared spectroscopy. A great similarity of the absorption spectra of the films in the main directions was observed, thus revealing a nearly perfect isotropy of the initial semi-crystalline structures. The PE films displayed a slight orthotropy as compared to PA6, but no particular difference has been pointed out between the two in-plane directions. Moreover, the experimental results show a similar uniaxial behavior in any stretching direction for both PA6 and PE.

The global model encompassing all the behaviors revealed for each case previously presented is depicted in Fig. 8, in the style of a rheological model. Models for cases 1 and 2 are assumed to bear the same stress so that a series arrangement is retained. The model for case 3 initially corresponds to a much softer behavior which is paralleled with the others. The tangent modulus of case 3 is very weak in the first deformation stage as compared to the other two cases, whereas it is conversely predominant for larger strains. The configuration in Fig. 8 is the most adequate one, being able to predict the neglecting influence of case 3 and case 1-2 in the initial and advanced deformation stages, respectively. Moreover, due to the relative lengths of the different specimens (cases 1, 2 and 3), one may surely encounter a few samples of short and medium-sized chains aligned along each long chain of purely amorphous phase, in any arbitrary direction.

Based on the above remarks, the following relations can be deduced for the full model:

$$\begin{aligned}
&\boldsymbol{\Sigma}_{case1} = \boldsymbol{\Sigma}_{case2} \doteq \boldsymbol{\Sigma}_{case1-2} \\
&\boldsymbol{\Sigma}_{total} = \boldsymbol{\Sigma}_{case1-2} + \boldsymbol{\Sigma}_{case3} \\
&\boldsymbol{\varepsilon}_{case1-2} = \boldsymbol{\varepsilon}_{case1} + \boldsymbol{\varepsilon}_{case2} = \boldsymbol{\varepsilon}^e_{case1-2} + \boldsymbol{\varepsilon}^p_{case1-2} \\
&\boldsymbol{\varepsilon}_{total} = \boldsymbol{\varepsilon}_{case1-2} = \boldsymbol{\varepsilon}_{case3}
\end{aligned} \tag{11}$$

where $\boldsymbol{\Sigma}_{total}$ and $\boldsymbol{\varepsilon}_{total}$ are the global stress and strain tensors for the whole model, and $\boldsymbol{\Sigma}_{case}$ and $\boldsymbol{\varepsilon}_{case}$ correspond to the stresses and strains supported by one or two associated cases. The superscripts $.^e$ and $.^p$ stand for the elastic and plastic parts of the strain tensor. As previously explained, the elastic behaviors of cases 1 and 2 will not be particularized and a unique Young's modulus $E_{1-2} = E_1E_2/(E_1 + E_2)$ will be used for the serial arrangement, in the framework of the Saint–Venant–Kirchhoff linear elastic theory. Let us mention that this model will be implemented within the context of a plane stress formulation, for thin films applications. It means that $\boldsymbol{\Sigma}_{total}$ must verify the plane stress condition. For simplicity purposes, we assume that both $\boldsymbol{\Sigma}_{case\,1-2}$ and $\boldsymbol{\Sigma}_{case\,3}$ have a null transverse normal component. This approximation is not so detrimental since case 1-2 plays first a major role in the range of small deformations (case 3 is then insignificant), and case 3 is in turn the most predominant for larger strains.

It can be noticed that the proportion of each phase, which is related to the crystallinity of the material, does not explicitly appear in the model, but it is indirectly taken into account in the respective model parameters. For example, a Young's modulus is only defined for the combination of cases 1 and 2 and not for each single case, and it takes implicitly into consideration the volume fraction of each phase. Only such global parameters are needed to simulate the macroscopic behavior and they can be easily derived from experimental tests, contrary to the intrinsic

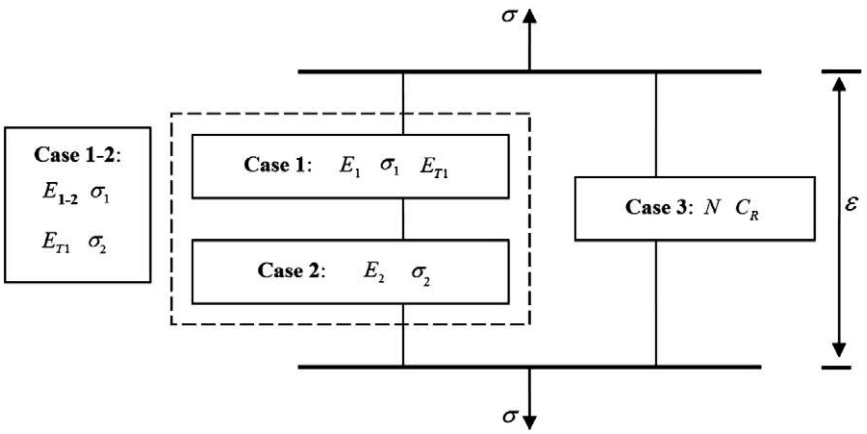

Fig. 8. Global representation of the mechanical model for semi-crystalline polymers.

moduli of each phase. Moreover, it allows us to define a simpler expression of the model with very few parameters, which is valid for any crystallization conditions (only the numerical values of the material parameters are changing).

4.3. Computation of the model parameters from uniaxial tests

The procedure involved for the determination of the model parameters is explained throughout the example of PA6. The corresponding uniaxial experimental curve is plotted in Fig. 9.

As shown in Fig. 8, cases 1 and 2 may be formally put together, giving rise to a unified set of elastoplastic coefficients, namely E_{1-2}, E_{T1}, σ_1 and σ_2.

In Fig. 9, the first two parts of the curve (for $0 \leqslant \varepsilon \leqslant \varepsilon_A$ and $\varepsilon_A \leqslant \varepsilon \leqslant \varepsilon_B$, respectively) are assumed to be linear, and their respective slopes E and H are obtained by linear regression with a reasonable correlation coefficient. For $\varepsilon \geqslant \varepsilon_B$ in the vicinity of ε_B (while strains remain moderate), the response curve is also quite linear, so that a third slope E_0 can be deduced again by linear regression, which corresponds to the initial elastic modulus of case 3.

First, the four parameters of case 1-2 are derived from the experimental curve using the following relations:

$$\begin{aligned} E_{1-2} &= E - E_0 \\ E_{T1} &= H - E_0 \\ \sigma_1 &= \sigma_A - E_0\varepsilon_A \\ \sigma_2 &= \sigma_B - E_0\varepsilon_B \end{aligned} \tag{12}$$

Then, C_R and N are determined as in Bergström and Boyce (1998). From the maximum strain ε_{lim} deduced from the uniaxial experimental curve by extrapolation, the limit stretch value is straightforward $\lambda_{lim} = \exp(\varepsilon_{lim})$, and one obtains:

$$N = \frac{1}{3}\left(\lambda_{lim}^2 + \frac{2}{\lambda_{lim}}\right) \tag{13}$$

Using an arbitrary point $(\varepsilon_t, \sigma_t)$ on the stress–strain curve, with $\lambda_{eq} = \exp(\varepsilon_t)$ and $\sigma_{eq} = \sigma_t - \sigma_2$, one finally gets:

$$C_R = \frac{\sigma_{eq}}{\lambda_{eq}^2 - \frac{1}{\lambda_{eq}}} \sqrt{\frac{\lambda_{eq}^2 + \frac{2}{\lambda_{eq}}}{3N}} \left[\mathscr{L}^{-1}\left(\sqrt{\frac{\lambda_{eq}^2 + \frac{2}{\lambda_{eq}}}{3N}}\right)\right]^{-1} \tag{14}$$

Remark. The global behavior is assumed to be almost incompressible. Indeed, when large elastoplastic strains are involved, both models in parallel (1–2 and 3) display such a behavior. On one hand (case 1–2), the elastic strains are negligible, and the von Mises type criteria used imply an incompressible plastic behavior. On the other hand, the eight-chain model is consistent with this hypothesis. On the contrary, for particularly small strains, the global behavior is governed by the elastic part of case 1-2 (considering that stresses in the amorphous phase are relatively small, as compared to those concerning the two other cases in series). A Poisson coefficient ν can thus be simply derived for this model as the ratio between the transverse strain and the longitudinal one in the onset of the uniaxial test:

$$\nu = -\frac{\varepsilon_{trans}}{\varepsilon_{long}} \tag{15}$$

The numerical value obtained is not so far from 0.5 (elastic strains are also nearly incompressible), and most of all, it only concerns very small strains so that the effect of the Poisson's ratio can be neglected in most of the strain range considered. The apparent contradiction between a slightly compressible material and a perfectly incompressible model in parallel is not an issue since only bi-dimensional strains and stresses are further considered within the plane stress formulation retained.

5. Simulation results: validation and analysis

The procedure discussed above is applied to the uniaxial experimental curves obtained for PA6 and PE. Once the

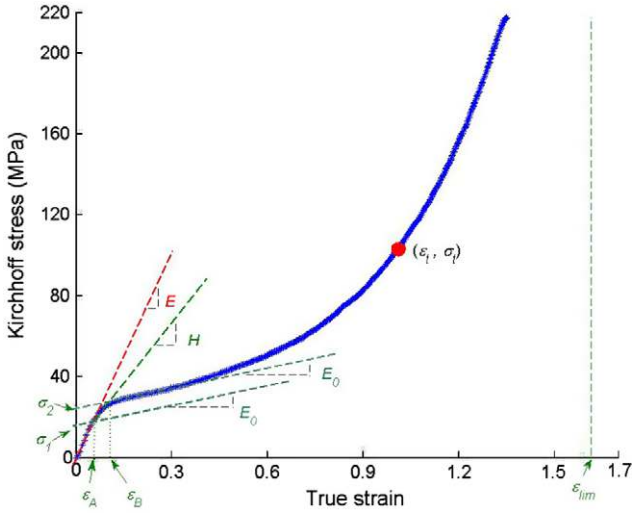

Fig. 9. Calculation of the model parameters for PA6 using the uniaxial curve.

model parameters are known, it is possible to simulate the mechanical behavior of PA6 and PE films under uniaxial or equi-biaxial drawing, and compare the numerical solutions to the corresponding experimental results (Sallem-Idrissi et al., 2009). On one hand, a very good agreement between both experimental and numerical curves is expected in the uniaxial case, since material parameters were chosen in order to closely fit the uniaxial test response. On the other hand, the biaxial results are supposed to validate the previous formulation used for this type of material.

For PA6, the following parameters are identified according to Fig. 9: σ_1 = 11.8 MPa, σ_2 = 21.7 MPa, E_{1-2} = 431 MPa, N = 9.17, C_R = 7.34 MPa, E_{T1} = 121 MPa, ν = 0.44.

As expected, in Fig. 10, the uniaxial simulation results fit the experimental results very well. In the biaxial case, simulation results are also in good agreement with the corresponding experimental results. The slightly higher values obtained with the model may be due to the slight anisotropy of PA6 which is not taken into account. The mechanical properties of PA6 used in the biaxial simulation are derived from uniaxial tests performed in the strongest direction of the material sheet.

In the case of PE, the testing temperature (90 °C) is closer to the melting temperature of the material (see Table 1). As a consequence, the stress–strain curve of PE (see Fig. 11) is slightly different compared to that of PA6. Under such a temperature, the yielding stresses of cases 1 and 2 are very near one from each other, and the "viscous" effects may be not negligible yet. It may be induced by the slipping of chains in case 1, that makes the curve not so fluent than in Fig. 9. As shown in Fig. 11, each continuous part of the curve which presents almost the same hardening slope E_{T1} (see Section 4.1.1) is followed by a stress softening phenomenon.

For comparison purposes, Fig. 12 depicts the uniaxial experimental stress–strain behavior of PE at a much lower temperature, which seems to present a similar tendency as for PA6 (the two yielding points are more distinguishable).

In spite of these differences, one can obtain the following parameters in a quite similar way: σ_1 = 0.88 MPa, σ_2 = 1.6 MPa, E_{1-2} = 18.1 MPa, N = 49.5, C_R = 1.18 MPa, E_{T1} = 9.2 MPa, ν = 0.39.

Fig. 13 displays both numerical and experimental curves of PE in uniaxial and equi-biaxial drawing. From small up to moderate strains, the simulation results fit the experimental ones very well. When the strains become much larger, the two curves slightly differ due to the strain softening phenomena.

Finally, it is interesting to remark that, despite an initially isotropic behavior, induced anisotropy may occur, due to the large elastoplastic strains and to the microstructure of the materials, especially after successive elastic unloading and plastic reloading. Our model naturally involves such a phenomenon, because of the global arrangement of the three phases. Moreover, to some extent, the adequacy of the experimental and simulation unloading curves in Fig. 14 corroborates the fact that the evolution of anisotropy is well-depicted.

6. Conclusion

In this paper, a specific elastoplastic constitutive model is developed for semi-crystalline polymers in the framework of isothermal transformations (between the glass transition and the melting temperatures) under low-level strain rates, so that viscosity effects are not considered. Based on the analysis of the structural morphology of semi-crystalline polymers from a mesoscopic point of view, three cases are considered, depending on the distance between crystalline blocks. A particular model is proposed for each configuration, namely small (1), medium-sized (2) and large (3) amorphous regions. For case 1, a classical elastoplastic model is retained. For case 2, a perfect plastic model is suggested with a new threshold stress, defined using a "multi-axial factor" as a function of the deformation state. For case 3, the so-called "eight-chain" model is employed. The intermediate case mainly describes the sliding phenomenon between entangled chains and is capable to explain the most significant features of the experimental behavior.

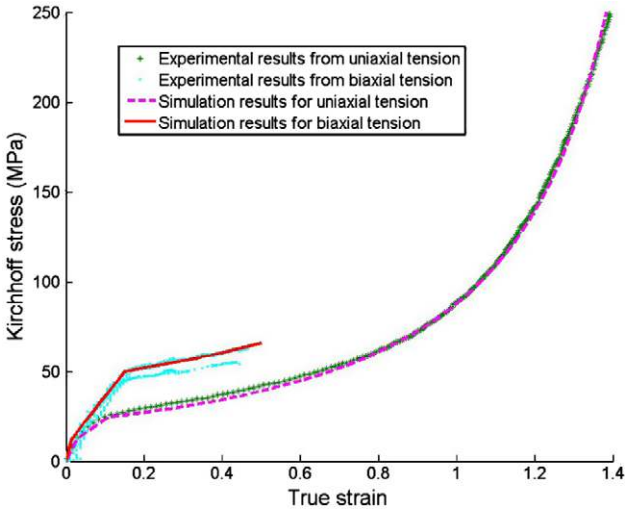

Fig. 10. Comparisons between simulation and experimental results for PA6 at 90 °C in both uniaxial and equi-biaxial cases.

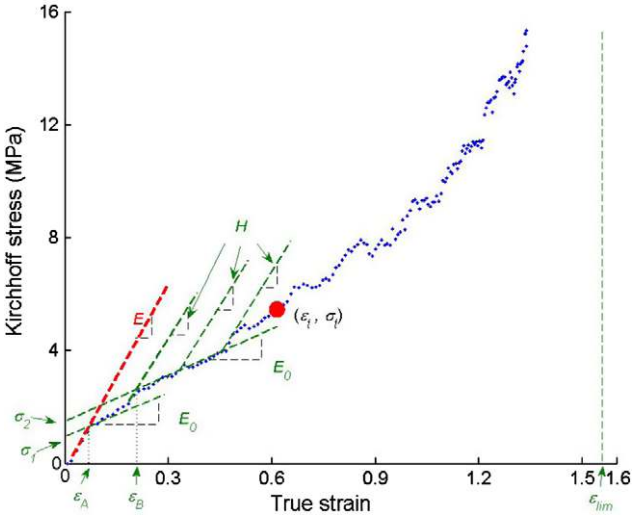

Fig. 11. Calculation of the model parameters for PE using the uniaxial curve.

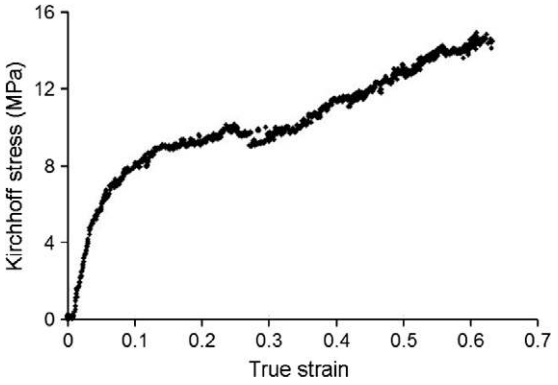

Fig. 12. Experimental uniaxial stress–strain curve of PE at 20 °C.

A global constitutive model is then built by properly assembling the three components above, displaying only seven material parameters. A methodology for the calibration of these parameters from uniaxial tests is presented and applied in the case of PA6 and PE.

Once the models defined, simulations are performed also in equi-biaxial stretching and numerical results agree very well with the experimental ones. Large discrepancies only appear during unloading, when it takes place at high stress values, in the vicinity of null stresses (when the load vanishes). Therefore, this model describes properly the arbitrary behavior of such a polymer film in plane stresses, once strain rates are not too high and unloading is not too strong or just restricted to a small area.

The constitutive model developed in this study has thus proved to be able to reproduce the biaxial behavior according to parameters calibrated from uniaxial tests, for two different semi-crystalline polymers. The next step can now be undertaken, namely the identification of the correlation between the model parameters and

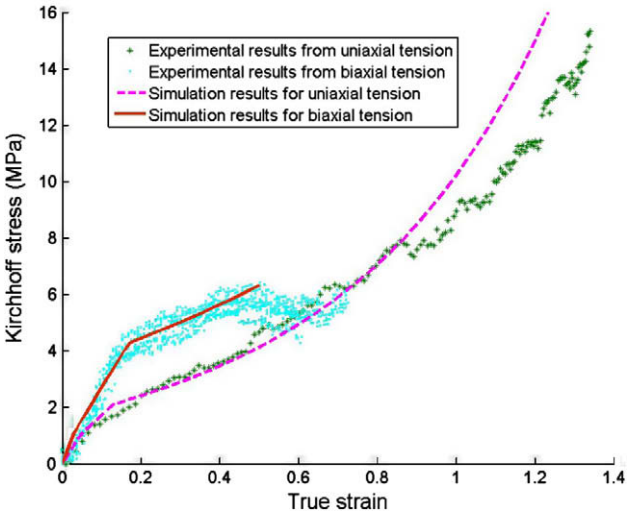

Fig. 13. Comparisons between simulation and experimental results for PE at 90 °C in both uniaxial and equi-biaxial cases.

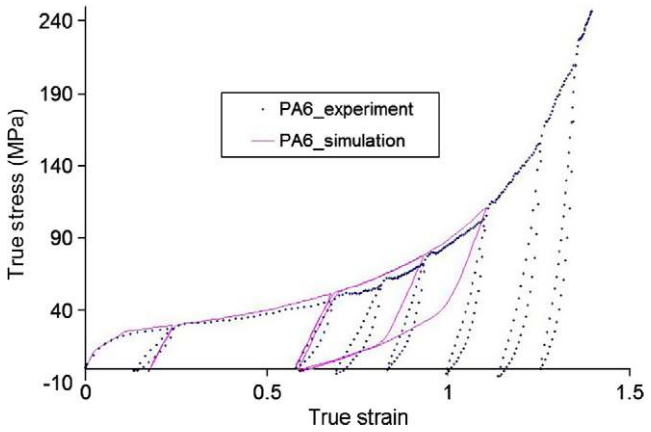

Fig. 14. Comparisons between simulation and experimental results during unloading in the uniaxial case.

characteristic quantities describing the crystalline morphology of the considered polymers.

Acknowledgements

Thanks are due to Conseil Régional (Regional Council) Nord-Pas-de-Calais, France, and the European Union (European Funds for Regional Development, FEDER) for having partly funded the video-traction equipment. DSM and SABIC are also deeply acknowledged for the PA6 and PE raw materials. The authors also wish to thank Naïma Sallem-Idrissi for her biaxial stretching experiments.

References

Aboulfaraj, M., G'Sell, C., Ulrich, B., Dahoun, A., 1995. In situ observation of the plastic deformation of polypropylene spherulites under uniaxial tension and simple shear in the scanning electron microscope. Polymer 36 (4), 731–742.

Arruda, E.M., Boyce, M.C., 1993. A three-dimensional constitutive model for the large stretch behavior of rubber elastic materials. Journal of the Mechanics and Physics of Solids 41 (2), 389–412.

Balsamo, V., Müller, A.J., 1993. The phenomenon of double yielding under tension in low-density polyethylene, linear low-density polyethylene and their blends. Journal of Materials Science Letters 12 (18), 1457–1459.

Bergström, J.S., Boyce, M.C., 1998. Constitutive modeling of the large strain time-dependent behavior of elastomers. Journal of the Mechanics and Physics of Solids 46 (5), 931–954.

Bergström, J.S., Kurtz, S.M., Rimnac, C.M., Edidin, A.A., 2002. Constitutive modeling of ultra-high molecular weight polyethylene under large-deformation and cyclic loading conditions. Biomaterials 23 (11), 2329–2343.

Boni, S., G'Sell, C., Weynant, E., Haudin, J.M., 1982. Microscopic in situ observation of the plastic deformation of polybutene-1 films under simple shear. Polymer Testing 3 (1), 3–24.

Diani, J., Brieu, M., Vacherand, J.M., Rezgui, A., 2004. Directional model for isotropic and anisotropic hyperelastic rubber-like materials. Mechanics of Materials 36 (4), 313–321.

Drozdov, A.D., Christiansen, J. de C., 2008. Thermo-viscoelastic and viscoplastic behavior of high-density polyethylene. International Journal of Solids and Structures 45 (14–15), 4274–4288.

Dupaix, R.B., Boyce, M.C., 2007. Constitutive modeling of the finite strain behavior of amorphous polymers in and above the glass transition. Mechanics of Materials 39 (1), 39–52.

Elías-Zúñiga, A., Beatty, M.F., 2002. Constitutive equations for amended non-Gaussian network models of rubber elasticity. International Journal of Engineering Science 40 (20), 2265–2294.

Fatahi, S., Ajji, A., Lafleur, P.G., 2007. Correlation between different microstructural parameters and tensile modulus of various polyethylene blown films. Polymer Engineering and Science 47 (9), 1430–1440.

Feijoo, J.L., Sanchez, J.J., Müller, A.J., 1997. The phenomenon of double yielding in oriented high density polyethylene films. Journal of Materials Science Letters 16 (21), 1721–1724.

Gueguen, O., Richeton, J., Ahzi, S., Makradi, A., 2008. Micromechanically based formulation of the cooperative model for the yield behavior of semi-crystalline polymers. Acta Materialia 56 (7), 1650–1655.

Heck, B., Hugel, T., Iijima, M., Strobl, G., 2000. Steps in the formation of the partially crystalline state. Polymer 41 (25), 8839–8848.

Hong, K., 2005. A Model Treating Tensile Deformation of Semi-crystalline Polymers. Ph.D. Thesis, Albert-Ludwigs-Universität Freiburg im Breisgau.

Hong, K., Rastogi, A., Strobl, G., 2004. A model treating tensile deformation of semi-crystalline polymers: quasi-static stress–strain relationship and viscous stress determined for a sample of polyethylene. Macromolecules 37 (26), 10165–10173.

James, H.M., Guth, E., 1943. Theory of the elastic properties of rubber. Journal of Chemical Physics 11 (10), 455–481.

Kuhn, W., Grün, F., 1942. Beziehungen zwischen elastischen Konstanten und Dehnungsdoppelbrechung hochelastischer Stoffe. Kolloid-Zeitschrift 101 (3), 248–271.

Lee, B.J., Argon, A.S., Parks, D.M., Ahzi, S., Bartczak, Z., 1993. Simulation of large strain plastic deformation and texture evolution in high density polyethylene. Polymer 34 (17), 3555–3575.

Mandelkern, L., 2006. Crystalline polymer: some reminiscences over the years. Thermochimica Acta 442 (1–2), 31–34.

Miehe, C., Göktepe, S., Lulei, F., 2004. A micro–macro approach to rubber-like materials – Part I: The non-affine micro-sphere model of rubber elasticity. Journal of the Mechanics and Physics of Solids 52 (11), 2617–2660.

Peacock, A.J., 2000. Handbook of Polyethylene: Structures Properties and Applications. Marcel Dekker.

Richeton, J., Ahzi, S., Vecchio, K.S., Jiang, F.C., Makradi, A., 2007. Modeling and validation of the large deformation inelastic response of amorphous polymers over a wide range of temperatures and strain rates. International Journal of Solids and Structures 44 (24), 7938–7954.

Sallem-Idrissi, N., 2008. Comportement mécanique et évolution structurale induite dans les films multi-couches à base de polyamide 6 et de polyéthylène. Ph.D. Thesis, Université des Sciences et Technologies de Lille/Ecole des Mines de Douai.

Sallem-Idrissi, N., Miri, V., Elkoun, S., Krawczak, P., Lacrampe, M.F., Lefebvre, J.M., Séguéla, R., 2009. Trichroic infrared analysis of the strain-induced structural changes in the PA6 layer of PA6/PE multilayer films under biaxial drawing. Polymer 50 (24), 5812–5823.

Séguéla, R., Rietsch, F., 1990. Double yield point in polyethylene under tensile loading. Journal of Materials Science Letters 9 (1), 46–47.

Shan, G.F., Yang, W., Xie, B.H., Li, Z.M., Chen, J., Yang, M.B., 2005. Double yielding behaviors of polyamide 6 and glass bead filled polyamide 6 composites. Polymer Testing 24 (6), 704–711.

van Dommelen, J.A.W., Parks, D.M., Boyce, M.C., Brekelmans, W.A.M., Baaijens, F.P.T., 2003. Micromechanical modeling of the elasto-viscoplastic behavior of semi-crystalline polymers. Journal of the Mechanics and Physics of Solids 51 (3), 519–541.